Thresholds for post-rebound viral control after CCR5 gene-edited autologous hematopoietic cell transplantation

E. Fabian Cardozo[1], Elizabeth R. Duke[1,3], Christopher W. Peterson[2,3], Daniel B. Reeves[1], Bryan T Mayer[1], Hans-Peter Kiem[2,3,4], Joshua T. Schiffer[1,2,3,*]

[1]Vaccine and Infectious Disease Division,

[2]Clinical Research Division, Fred Hutchinson Cancer Research Center, Seattle, WA, USA;

[3]Department of Medicine and

[4]Department of Pathology, University of Washington, Seattle, WA, USA.

*Corresponding Author

Short title: Post-rebound SHIV control after ΔCCR5 HSPC transplantation

Abstract (248/250 words)

Two recent cases of HIV cure/stable remission following allogeneic stem cell transplantation are difficult to reproduce because of inherent toxicities and the rarity of donors homozygous for the CCR5Δ32 deletion. One approach to overcome these barriers and improve safety is the use of autologous, CCR5 gene-edited hematopoietic stem and progenitor cell (HSPC) products. Unlike allogeneic transplantation, in which the frequency of CCR5Δ32 donor cells approaches 100%, the CCR5 gene can currently only be edited in a fraction of autologous HSPCs. Therefore, we sought to determine the minimum fraction required for post-rebound viral control using mathematical modeling. We analyzed data from eight juvenile pigtail macaques infected intravenously with SHIV-1157ipd3N4, treated with combination antiretroviral therapy (cART), and infused with autologous HSPCs without CCR5 gene editing. We developed a mathematical model that simultaneously described reconstitution of $CD4^+$ $CCR5^+$, $CD4^+$ $CCR5^-$, and $CD8^+$ T cell counts, as well as SHIV plasma viral loads in control and transplanted macaques. By modifying the model to hypothetically describe transplant with some fraction of protected CCR5-edited cells, we found that transplantation had differential effects on the macaques' immunologic control of SHIV: those with a loss of immunologic control had a more profound depletion of $CCR5^+CD4^+$ T cells and would require higher fractions of gene-edited cells (~97%) than those that maintained immunologic control (~60%). Our results provide a framework to predict the likelihood of post-rebound control *in vivo,* based on the percentage of CCR5-edited cells in peripheral blood and the loss of HIV-specific immunity following autologous HSPC.

(Main text: 3789/4000 words, including headings)

INTRODUCTION

The major obstacle to HIV-1 eradication is the latent reservoir of long-lived infected cells[1-3]. Cure strategies aim to eliminate all infected cells or prevent sustained viral reactivation from latency. The only known case of HIV cure[4,5] and an additional, recently-reported case of prolonged remission[6], resulted from allogeneic hematopoietic stem cell transplant with homozygous CCR5Δ32 donor cells[4-6]. The success of this procedure is likely multifactorial—in part attributable to HIV resistance of the transplant product, the conditioning regimen that facilitates engraftment, some graft-versus-host effect, and immunosuppressive therapies for graft-versus-host disease[7-11].

A current research focus is to recapitulate this method of cure with minimal toxicity. One method is to perform autologous transplantation following ex vivo editing of the CCR5 gene with a zinc finger nuclease, eliminating the need for allogeneic CCR5-negative donors[12,13]. While this procedure is safe and feasible in pigtail macaques infected with simian-human immunodeficiency virus (SHIV)[13-16], only a fraction of HSPCs can be genetically modified *ex vivo* to be HIV-resistant.

Due to this challenge, we developed a mathematical model that can be used to predict the minimum threshold of persisting, gene-modified cells necessary for functional cure. First, we modeled the kinetics of $CD4^+CCR5^+$, $CD4^+$ $CCR5^-$, and $CD8^+$ T cell reconstitution after autologous transplantation. We then modeled SHIV rebound kinetics following analytical treatment interruption (ATI) and identified the degree of loss of anti-HIV cytolytic immunity following transplantation. Finally, we projected the proportion of gene-modified cells and the levels of SHIV-specific immunity required to eliminate viral replication following ATI.

METHODS

Experimental Data

Eight juvenile pigtail macaques were intravenously challenged with 9500 TCID50 SHIV-1157ipd3N4 (SHIV-C)[14,17]. After 6 months, the macaques received combination antiretroviral therapy (cART: tenofovir [PMPA], emtricitabine [FTC], and raltegravir [RAL]). After ~25 weeks on cART, four animals received total body irradiation (TBI) followed by transplantation of autologous HSPCs. After an additional 25 weeks following transplant, when viral load was fully suppressed, animals underwent analytical treatment interruption (ATI)[14]. A control group of four animals did not receive TBI or HSPCs transplantation and underwent ATI after ~50 weeks of treatment (**Fig. 1A**). Plasma viral loads and absolute quantified $CD4^+CCR5^-$, $CD4^+CCR5^+$ and $CD8^+$ total and subsets (naïve, central memory [T_{CM}], and effector memory [T_{EM}]) T cell counts from peripheral blood were measured as described previously[14,17]. We analyzed peripheral T cell counts and plasma viral load from transplant until 43 weeks (~25 weeks pre-ATI and ~18 weeks post-ATI).

Mathematical modeling

We employed several series of ordinary differential equation models of cellular and viral dynamics after transplantation. First, we modeled T cell dynamics and reconstitution following transplant and before ATI, assuming that low viral levels do not affect cell dynamics (**Fig. 1B**). After curation of that model, we introduced viral dynamics and fit those to the T cell and viral rebound dynamics from the animals (**Fig. 1C**). Lastly, we used our complete model in a transplant scenario with gene editing of CCR5 to predict the minimal threshold of editing for functional HIV cure.

T cell reconstitution after transplantation: We modeled the kinetics of $CD4^+$ and $CD8^+$ T cell subsets in blood, transplanted cells that home to the BM, and progenitor cells in the BM/thymus as shown in **Fig. 1B**. We included $CD8^+$ T cells in the model because $CD8^+$ and $CD4^+$ T cells may arise from new naïve cells from the thymus and compete for resources that impact clonal expansion and cell survival[18-20]. At the moment of HSPC infusion, transplanted animals are lymphopenic due to TBI. The control group did not have a transplanted-cell compartment, and all other compartments remained in steady state. We assumed that $CD4^+$ and $CD8^+$ T cell expansion may have two possible drivers: (1) lymphopenia-induced proliferation of mature cells that persist through myeloablative TBI[18,21-25], and (2) differentiation from naïve cells from progenitors in the thymus (from transplanted $CD34^+$ HSPCs[26,27] or $CD34^+$ HSPCs that survive TBI) and further differentiation to an activated effector state[24,25,28-32]. We assumed that in a lymphopenic environment, factors that drive T cell proliferation are more accessible (i.e., self-MHC molecules on antigen-presenting cells[28,29,33,34] and γ-chain cytokines such as IL-7 and IL-15[21-23,35-37]). However, as they grow, cells compete for access to these resources, limiting clonal expansion[18] such that logistic growth models are appropriate[19]. We assume that new peripheral $CD4^+$ and $CD8^+$ T naïve cells come from a progenitor compartment in the BM/Thymus[38,39]. For $CD4^+$ T cells the models assume that naïve cells do not express CCR5[40-42], and subsequently up- and/or down-regulate expression of the CCR5 receptor[30]. For $CD8^+$ T cells we included a single $CD8^+$ memory precursor compartment of T_N and T_{CM} cells that differentiate linearly into T_{EM} during lymphopenia[43-45]. The details of the model are presented in the **Supp. Material** and in **Fig. 1B,** with the symbols described in **Table 1**. A parsimonious model based on the one

described above was selected from a series of models with varying statistical complexity as presented in the **Supp. Materials.**

T cell and viral dynamics: We adapted the previous model combining several adaptations of the canonical model of viral dynamics[43-53] as shown in **Fig. 1C**. The model assumes that SHIV only infects $CD4^+CCR5^+$ T cells[17], and that only a small fraction (~ 5%) of those infected cells are able to produce infectious virus[51,54,55]. We modeled cART by reducing infection rate to zero, and modeled ATI by assuming infection is greater than zero after some time Δ_t after interruption. This model assumes also that productively infected cells arise also from activation of a steady set of latently infected cells. The presence of both unproductively and productively infected cells leads to the expansion of $CD8^+$ $T_{naïve}$ and T_{CM} cells, from which the majority of dividing cells differentiate into SHIV-specific effector cells[30,46,47,52,53]. The details of the model are presented in the **Supp. Material** and in **Fig. 1C,** with the symbols described in **Table 1**. A parsimonious model based on the one described above was selected from a series of models with varying statistical complexity as presented in the **Supp. Materials.**

Viral and T cell dynamics in the setting of ΔCCR5 HSPC transplantation: We next adapted our model to simulate scenarios in which autologous transplantation includes cells that are CCR5-edited. We added variables representing CCR5-edited HSPCs, T cell progenitors in BM/thymus, and $CD4^+CCR5^-$ T cells in blood. These compartments have the same structure as CCR5-non-edited cells but with two differences. First, the value of HSPCs at transplantation is a fraction f_p of the total number of infused cells, i.e. representing the proportion of infused HSPCs that were

CCR5-edited. Second, mature $CD4^+CCR5^-$ cells with CCR5 edition do not upregulate CCR5 (see full model in **Supp. Materials**).

Fitting procedure and model selection

We used a nonlinear, mixed-effects modeling approach[56] described in detail in **Supp. materials**. Briefly, parameters for individual animals were sampled from a probabilistic model that describes the population with a fixed effect or population median, and a random effect with a standard deviation that describes the parameter variability in the population. We first fit instances of the model in **Fig. 1B** to blood T cell counts during transplant and before ATI (**Table S1** includes all 19 competing models). Then, we fit several instances of the model **Fig. 1C** to blood T cell counts and plasma viral load during the period after transplant including ATI, using the best competing model for the model in **Fig. 1B** (**Table S2** includes all 15 competing models). For each step we fit each competing model to all data points from all animals simultaneously using a maximum likelihood approach. We estimated the standard deviation of the measurement error for the observations, and each parameter fixed effects and standard deviation of the random effects using the Stochastic Approximation of the Expectation Maximization (SAEM) algorithm embedded in the Monolix software (www.lixoft.eu)[56]. For best fit of the different possible versions of the models we computed the log-likelihood (log L) and the Akaike Information Criteria (AIC=-2log L+2m, where m is the number of parameters estimated)[57] to obtain the most parsimonious model. We assumed a model has similar support from the data if the difference between its AIC and the best model (lowest) AIC is less than two[57] (see **Supp. materials** for details).

RESULTS

$CD4^+CCR5^+$ and $CD8^+$ T cells recover more rapidly than $CD4^+CCR5^-$ T cells after HSPC transplantation. We analyzed the kinetics of peripheral blood $CD4^+CCR5^+$ and $CD4^+CCR5^-$ T-cells, and total, $T_{naïve}$, T_{CM}, and T_{EM} $CD8^+$ T-cells in macaques after HSPC transplantation (**Fig. 1A**). In controls, levels of $CD4^+$ and $CD8^+$ T cells oscillated around a persistent set point (blue lines in **Fig. 2A-C** and **Fig. S1A-B**). In the control group, $CD4^+$ $CCR5^+$ T cell levels were ~100 cells/μl and were uniformly lower than the $CD4^+CCR5^-$ T cell counts (~1200 cells/μl) ($p=0.01$, Paired t-test of the averaged measures post-transplant. See **Fig. 2D**). Total $CD8^+$ T cell levels in the control group were ~1400 cells/μl with a greater contribution from T_{EM} (73%) than T_N+T_{CM} (27%) (Based on median values. See **Fig. 2D**)**.** In the transplant group immediately post-TBI, the levels of $CD4^+CCR5^+$ T cells started at 1-10 cells/μl and reconstituted to levels similar to the control group over 5-10 weeks (**Fig. 2A**). After TBI, $CD4^+CCR5^-$ T cells remained at higher levels (~100 cells/μl) than $CD4^+CCR5^+$ T cells but expanded more slowly and did not reach the values of the control group after 25 weeks (**Fig. 2B**). The $CD4^+CCR5^+$ T cell compartment expanded 8-fold more rapidly than the $CD4^+CCR5^-$ compartment ($p=0.01$, Paired t-test. See **Fig. 2E**). Following TBI in the transplanted group, $CD8^+$ T cells decreased to levels between 10 and 100 cells/μl after TBI but recovered to levels below the control group in 5 weeks (**Fig. 2C**); these cells recovered as fast as the $CD4^+CCR5^+$ population (**Fig. 2E**). $CD8^+$ T cell levels were highly correlated with the $CD8^+$ T_{EM} subtype but not to the naïve or T_{CM} subtypes (**Fig. 2F** and **Figures S1C-D**). Overall, these results show that during post-transplantation there is a faster reconstitution of $CD4^+CCR5^+$ and $CD8^+$ T cells compared to $CD4^+CCR5^-$ cells, and that $CD8^+$ T cells are composed mostly of T_{EM}.

Lymphopenia-induced proliferation favors $CD4^+CCR5^+$ and $CD8^+$ T cell reconstitution after HPSC transplantation. To understand what are the main drivers of T cell reconstitution we developed a mathematical model that included the plausible mechanisms underlying differing T cell subsets reconstitution following autologous transplantation (**Fig. 1B**). We built 19 versions of that model by assuming that one or multiple mechanisms are absent, or by assuming certain mechanisms have equal kinetics (**Table S1**). Using model selection theory based on AIC, we identified the model in **Fig. 3A** which most parsimoniously reproduces the data (**Table S1**). The main features of this model are: (1) $CD4^+CCR5^+$ T cell reconstitution after transplant is driven by proliferation and upregulation of CCR5; (2) $CD4^+CCR5^-$ T cell expansion is driven only by new naïve cells from the thymus; and (3), thymic export rates are equal between $CD4^+$ and $CD8^+$ naïve T cells.

The best fits of this model are presented in **Figures S2-S3** and **Fig. 3B-E** with the respective parameter estimates in **Tables S3-S4**. The best fitted model predicts that $CD4^+CCR5^-$ T cells have a delayed reconstitution that occurs only when cells from the thymus (estimated with rate ~0.01/day) outnumber their loss during death, trafficking to tissues or upregulation of CCR5. Furthermore, the estimated $CD4^+CCR5^+$ T cell proliferation rate (~0.1/day) far exceed the estimated CCR5 upregulation (~0.004/day) and thymic export rates. Therefore, total cell proliferation in this cell compartment is predicted by the model to be up to 40-fold higher than the concentration of cells that up-regulate CCR5 **(Fig. 3F** and **Fig. S4)**.

Our model also predicts that $CD8^+$ T cells follow a similar pattern to $CD4^+CCR5^+$ T cells (**Fig. 3D-E**), with $CD8^+$ T_{EM} proliferation rate up to 10-fold higher than the $CD8^+$ T cell differentiation rate (**Fig. S4**). Overall, these results suggest that following autologous HSPC transplant: (1) slow thymic export is the main driver of $CD4^+CCR5^-$ T cell growth, and (2) rapid

lymphopenia-induced proliferation of remaining cells (rather than transplanted cells) after TBI is the main driver for $CD4^+CCR5^+$ and $CD8^+$ T cell expansion.

Reduction of blood $CD4^+CCR5^+$ T cell counts correlates with plasma viral rebound after ATI in animals that underwent HSPC transplantation. We next aimed to compare plasma viral load rebound kinetics to $CD4^+CCR5^+$ and $CCR5^-$ T cell subset dynamics after ATI, in the context of previous plasma viral load analyses that we have performed from these animals[14,51]. **Fig. 4A-C** presents the plasma viral loads and the blood $CD4^+CCR5^+$ and $CD4^+CCR5^-$ T cell counts before and after ATI. The median peak viral load after treatment interruption was 10-fold higher for the transplant group (p=0.06, Mann-Whitney test. See **Fig. 4D**). Similarly, the median of the final viral load measurements at necropsy was 2-$\log_{10}$ higher in the transplant group (p=0.06, Mann-Whitney test. See **Fig.4E**). $CD4^+CCR5^+$ T-cell counts decreased after ATI in the transplant group: nadir was significantly lower (~8-fold) than in the control animals (p=0.01, Mann-Whitney test. **Fig. 4F**). The maximum reduction of $CD4^+CCR5^+$ T cells occurred in the same two animals with the highest viral set points. There was no difference between control and transplant groups in the $CD4^+CCR5^-$ T cell compartment: both groups had an average of ~200 cells/μL (**Fig.4G**). None of the individual plasma viral load observations in the control group post-ATI did not correlate with the corresponding $CD4^+CCR5^+$ T-cell counts post-ATI. However, in three animals in the transplant group, viral load observations post-ATI correlated negatively with their corresponding $CD4^+CCR5^+$ T cell counts (**Fig. 4H**). On the other hand, plasma viral loads were negatively correlated with the $CD4^+CCR5^-$ T cell count in two animals in both the control and transplant groups (**Fig. S5**). These results suggest that autologous HSPC

transplantation (without gene editing) affects SHIV-infected macaques so that the presence of the virus leads to more depletion of $CD4^+CCR5^+$ T cells.

Higher viral set points and $CD4^+CCR5^+$ T-cell depletion following transplantation and ATI are due to a reduction in SHIV-specific immunity. To understand why transplantation may have an effect in virus and $CD4^+CCR5^+$ T cell kinetics during ATI, we modified our mathematical model to include SHIV infection as described in **Fig. 1C** (**Methods**). Using model selection theory based on AIC, we found that the most parsimonious model to explain the data was the one shown in **Fig. 5A** (**Table S2**). In the best fit model SHIV-specific $CD8^+$ effector cells reduce virus production in a non-cytolytic manner[58-60] (e.g. possibly by secretion of HIV-antiviral factors[61-64]—not included in the model). Finally, the model assumes that infection leads to enhanced activation of $CD4^+CCR5^-$ T cells leading to replenishment of $CD4^+CCR5^+$ T cells, explaining the concentration reduction of the $CD4^+CCR5^-$ compartment after ATI[65-68].

The model simultaneously recapitulates plasma viral rebound, and the kinetics of $CD4^+$ $CCR5^+$ and $CCR5^-$ T cells in each animal as shown in **Fig. 5B** and **Fig. S6-S7** with corresponding estimated parameters in **Table 1** and **Table S5-S6**. From the estimated parameters, only SHIV-based $CD8^+$ proliferation rate, ω_8, correlated with post-ATI viral load set point and $CD4^+CCR5^+$ T-cell nadir (**Fig. 5C-D**). We also found that the estimated SHIV-based $CD8^+$ proliferation rate (ω_8) was significantly lower in the transplant group, and the estimated time to viral rebound (Δ_t) was significantly higher in the transplant group (**Fig. 5E-F**). The projected fraction of SHIV-specific $CD8^+$ T cells in the transplant group approached zero (**Fig. S8**). Overall, these results suggest that HSPC transplantation may lead to varying degrees of loss

of the immune response to SHIV infected cells, in turn leading to higher viral loads and loss of $CD4^+CCR5^+$ T cells.

Greater loss of immunologic control during TBI/transplant requires higher numbers of CCR5-edited HSPCs to control viral rebound after ATI. To calculate the minimum threshold of CCR5-edited cells necessary to induce cART-independent virus suppression, we next added a population of transplanted, gene-edited CCR5 HSPCs to the model in equation 2. We assumed that in the infused product there is a fraction f_p of HSPCs that have a biallelically modified CCR5 gene. Hence, $CD4^+$ T-cells derived from these HSPCs should not express CCR5. In the model we added state variables for protected progenitors and $CD4^+CCR5^-$ T cells that cannot become $CD4^+CCR5^+$ T cells (**Fig. 6A**, full model in **Supp. Materials**). **Fig. 6B** depicts projections of the model using the best estimates from the fits of the model to transplanted animal Z09144**,** using six values of f_p. For this animal, an initial fraction of protected cells smaller or equal than 40% will not lead to post-rebound viral control after ATI, even after a year. However, it is possible to have a spontaneous post-rebound viral control at ~40 weeks and 10 weeks after ATI when f_p is 60% or greater than 80%, We then simulated the model using parameter values obtained from the best fit in the previous section for each animal in the transplant group using 100 values of f_p from zero to one (0-100% CCR5-edited HSPCs). The heatmaps in **Fig. 6C-F** show plasma viral load projections after 2 years after the start of ATI for different values of f_p. The model predicts that the minimum f_p to maintain post-rebound control for 2 years after ATI is higher for animals with lower estimated SHIV-specific immune response rates. Using parameters estimates from the two animals in the transplant group with lower viral setpoints, the minimum f_p for viral control was 35% and 19% (**Fig. 6E-F**). In contrast, for the other two animals the minimum f_p for viral

control was 56% and 97% (**Fig. 6C-D**). These model projections suggest that a larger loss of immunologic control during TBI/HSPC transplant requires a higher fraction of CCR5 gene-edited cells to control viral rebound after ATI.

The model also predicts that for some values of f_p it is possible to have two viral set points: an initial high viral set point in the first weeks after ATI and then a delayed ART-free viral remission (e.g. when f_p=60% in **Fig. 6B** and between 60% and 70% in **Fig. 6C**). Therefore, in some cases the viral load set point during the initial weeks after ATI might not be a sufficient surrogate to predict viral control further in the future. However, we found that for the simulations predicting a delayed viral remission, the maximum decrease of $CD4^+CCR5^+$ T cells during the first 10 weeks after ATI has a linear relationship with the minimum initial fraction of protected cells required to obtain post-rebound control after 2 years **(Fig. 6G)**. We repeated these projections by adding the estimated measurement error to the simulations and obtained similar results (**Fig. 6H**). Therefore, the maximum initial change in $CD4^+CCR5^+$ T cells 10 weeks after ATI might predict late viral control.

Discussion

Here we introduce a data-validated mathematical that to our knowledge is the first to simultaneously recapitulate SHIV viral loads, as well as $CD4^+$ and $CD8^+$ T cell count subsets. The model predicts that post-rebound viral control might be possible during autologous gene-edited HSPC transplantation if therapy achieves (1) a sufficient fraction of gene-protected, autologous HSPCs, and (2) maintenance or enhancement of SHIV-specific immune responses following transplantation. Specifically, the model predicts that increasing amounts of conditioning regimen-dependent depletion of the SHIV-specific immune response leads to a higher threshold of CCR5-gene-edited cells in the transplanted HSPC product required to obtain

stable, ART-free viral control. These results are consistent with the cure achieved by the Berlin patient who received transplant with 100% HIV-resistant cells after intense conditioning[4,5]. In the autologous setting where 100% CCR5 editing may not be feasible, adjunctive measures that augment virus-specific immunity, such as therapeutic vaccination, infusion of HIV-specific CAR T cells or use of neutralizing antibodies, may synergize with HSPC transplantation to achieve post-treatment control[11,69].

We systematically selected from a series of mathematical models to arrive at a set of equations that most parsimoniously explains the available data. We recapitulated (1) peripheral $CD4^+$ and $CD8^+$ T-cell subset reconstitution dynamics following transplant, and (2) T-cell dynamics and SHIV viral rebound following ATI. Before ATI, all animals suppressed plasma viral load below the limit of detection, allowing analysis of T cell reconstitution dynamics independent of virus-mediated pressure. At each step, we applied model selection theory to select the simplest set of mechanisms capable of explaining the observed data[57].

The best model predicts that the lack of complete elimination of lymphocytes by TBI prevents $CD4^+CCR5^-$ cells from predominating post-transplant: the rapid expansion of $CD4^+CCR5^+$ and $CD8^+$ T cells during the first few weeks after HSPC transplantation is most likely due to lymphopenia-induced proliferation of remaining cells after TBI via a thymus-independent pathway; the slower expansion of $CD4^+CCR5^-$ T cells is more likely due to thymic export of both transplanted and remaining cells. An important future research question will be to identify anatomic sites and mechanisms allowing activated $CD4^+CCR5^+$ to survive conditioning.

A challenge is that more intense conditioning may decrease remaining $CD4^+CCR5^+$ cells but will also lower SHIV specific immunity. We previously demonstrated the link between disruption of the immune response during transplant and increased magnitude of viral rebound

during treatment interruption[14,51]. Here we predict that the magnitude of the SHIV-specific immune response is correlated not only with viral load set point, but also with the reduction of $CD4^+CCR5^+$ T cells after ATI. $CD4^+CCR5^+$ T cell depletion might be predictive of the loss of depletion of virus-specific immunity following conditioning.

A final important observation from the model is that viral control may be delayed beyond the first ten weeks after ATI, rather occurring after many months of treatment interruption. Thus, viral load levels during the initial weeks after ATI may not completely define success (stable ART-free remission), whereas $CD4^+CCR5^+$ T-cell nadir should more strongly correlate with the degree of depletion of virus-specific immunity. In this sense, minimal $CD4^+CCR5^+$ T-cell nadir may predict post-rebound viral control, if the starting fraction of protected cells is known.

Our results are limited by a small sample size of eight animals. For that reason, several model parameters were assumed to be the same among the population (i.e., without random effects). However, the number of observations for each animal was large enough to discriminate among different plausible model candidates. Therefore, we performed projections using only the individual estimated parameters. Reassuringly, our results align with prior mechanistic studies of cellular reconstitution after stem cell transplantation[18,26,38,70,71]. Our analysis also suggests that the majority of reconstituting $CD4^+CCR5^-$ T cells do not proliferate and have a slow expansion that concurs with estimates of thymic export from previous studies[26,70,71].

While our work highlights the complexity of the interplay between reconstituting HIV susceptible $CD4^+$ T cells, HIV-resistant $CD4^+$ T cells, infected cells, virus-specific immune cells, and replicating virus following autologous, CCR5-edited HPSC transplantation, our results illustrate the capabilities of modeling to glean insight from such a complex system. A

comprehensive understanding of these and similar systems will be required to optimize strategies for pre-clinical HIV cure studies, both in the macaque model, as well as in HIV^+ individuals.

Acknowledgements

This study was supported by grants from the National Institutes of Health, National Institute of Allergy and Infectious Diseases (UM1 AI126623). ERD is supported by the National Center for Advancing Translational Sciences of the National Institutes of Health under Award Number KL2 TR002317. DBR is supported by a Washington Research Foundation postdoctoral fellowship, and a CFAR NIA P30 AI027757. The funders had no role in study design, data collection and analysis, decision to publish, or preparation of the manuscript. The content is solely the responsibility of the authors and does not necessarily represent the official views of the National Institutes of Health or the Washington Research Foundation.

Disclosure of conflicts of interest

The authors declare no competing financial interests.

Animal welfare.

The data used in this work were collected in strict accordance with the recommendations in the *Guide for the Care and Use of Laboratory Animals* of the National Institutes of Health. The study protocol was approved by the Institutional Animal Care and Use Committees (3235-03) of the Fred Hutchinson Cancer Research Center and the University of Washington.

Tables

Table 1. Parameters of the model. Values are from steady state equations, using population estimates from best model fits or assumed from the references as described. When assumed from steady state equations, population estimates were used. See **Supp. Materials** for more details.

Parameter	Units	Description	Value		Source
			Control	Transplant	
$\boldsymbol{T(t_0)}$	cells	Number of cells in the transplant product.	0	$4*10^7$	Fixed, assumed from reference [14].
$\boldsymbol{P(t_0)}$	cells	Number of cells in the BM/Thymus at the moment of transplant.	$4*10^8$	0	Control: Computed from the median of steady state equations. Transplant: Fixed, assumed.
$\boldsymbol{N(t_0)}$	cells/μL	Blood $CD4^+CCR5^-$ T cell concentration at the moment of transplant.	1249	47	Control: Computed from the median of steady state equations. Transplant: Fitted.
$\boldsymbol{S(t_0)}$	cells/μL	Blood $CD4^+CCR5^+$ T cell	115	2	Control: Computed from

		concentration at the moment of transplant.			the median of steady state equations. Transplant: Fitted.
$\boldsymbol{M(t_0)}$	cells/μL	Blood $CD8^+$ T_N + T_{CM} cell concentration at the moment of transplant.	305	8	Control: Computed from the median of steady state equations. Transplant: Fitted.
$\boldsymbol{E(t_0)}$	cells/μL	Blood $CD8^+$ T_{EM} cell concentration at the moment of transplant.	935	17	Control: Computed from the median of steady state equations. Transplant: Fitted.
$\boldsymbol{E_h(t_0)}$	cells/μL	Blood SHIV-specific $CD8^+$ T effector cell concentration at the moment of transplant.	0	0	Control: Computed from steady state equations. Transplant: Assumed.
$\boldsymbol{I_p(t_0)}$	cells/μL	Productively infected blood $CD4^+CCR5^+$ T cell concentration at the	$2*10^{-6}$	$2*10^{-6}$	Computed from steady state equations.

		moment of transplant.			
$\boldsymbol{I_u(t_0)}$	cells/μL	Unproductively infected blood $CD4^+CCR5^+$ T cell concentration at the moment of transplant.	0	0	Computed from steady state equations.
$\boldsymbol{V(t_0)}$	RNA copies/mL	Plasma viral load at the moment of transplant.	0.5	0.5	Computed from steady state equations.
$\boldsymbol{k_e}$	1/day	Homing rate of transplanted cells into the bone marrow.	1		Fixed, assumed from references [72,73].
$\boldsymbol{\hat{r}_p = r_p - \lambda_p - d_p}$	1/day	Renewal rate of stem and progenitor cells in the bone marrow/thymus.	0.04		Fitted.
$\boldsymbol{\hat{r}_s = r_s - d_s}$	1/day	Proliferation rate of blood $CD4^+CCR5^+$ T cells.	0.14		Fitted.
$\boldsymbol{\hat{r}_m = r_m - \lambda_m - d_m}$	1/day	Proliferation rate of blood $CD8^+$ T_N + T_{CM} cells.	0.003		Fitted.

$\hat{r}_e = r_e - d_e$	1/day	Proliferation rate of $CD8^+$ T_{EM} cells.	0.09	Fitted.
$\hat{d}_n = \lambda_n + d_n$	1/day	Removal rate of blood $CD4^+CCR5^-$ T cells.	0.01	Fitted.
$\lambda_p = \lambda_e = \lambda_f$	1/day	Thymic output rate of T cells.	0.01	Fitted.
λ_n	1/day	CCR5 upregulation rate in $CD4^+$ T cells.	0.004	Fitted.
λ_m	1/day	Differentiation rate of $CD8^+$ T_N + T_{CM} cells to $CD8^+$ T_{EM} cells.	0.09	Fitted.
$K_p = K\frac{\hat{r}_p}{r_p}$	cells/μL	Effective carrying capacity of progenitor cells.	1664	Fitted.
$K_s = K\frac{\hat{r}_s}{r_s}$	cells/μL	Effective carrying capacity of $CD4^+CCR5^+$ T cells.	1328	Fitted.
$K_m = K\frac{\hat{r}_m}{r_m}$	cells/μL	Effective carrying capacity of $CD8^+$ T_N + T_{CM} cells.	49	Fitted.

$K_e = K\frac{\hat{r}_e}{r_e}$	cells/μL	Effective carrying capacity of $CD8^+$ T_{EM} cells.	1257	Fitted.
β	μL/ copies/day	Infectivity rate.	0.0003	Fitted.
Δ_t	days	Time to rebound after ATI.	7.5	Fitted.
δ_I	1/day	Death rate of infected $CD4^+CCR5^+$ T cells.	1	Fixed, assumed using estimates from references [74,75].
τ	-	Fraction of infected cell that produce infectious virus.	0.05	Fixed, assumed from reference [54].
$\xi\bar{L}$	cells/μL/day	Number of latent cells that activate per day.	$2*10^{-7}$	Fixed, assumed to have a viral load of ~0.5 copies/mL during cART.
π	1/day	Viral production rate.	$5*10^4$	Fixed, assumed using estimates from reference [76].
γ	1/day	Virus clearance rate.	23	Fixed, assumed using estimates from reference [77].
ω_4	μL/cells/day	SHIV-dependent replenishment of	0.19	Fitted.

		$CD4^+CCR5^+$ T cells.		
$\boldsymbol{\omega_8}$	μL/cells/day	SHIV-dependent proliferation rate of $CD8^+$ T cells.	0.002	Fitted.
$\boldsymbol{I_{50}}$	cells/μL	50% maximum value of adaptive infected cells, allows bounded growth.	0.20	Fitted.
$\boldsymbol{f}$	-	Fraction of SHIV-$CD8^+$-responding cells that become SHIV-specific effectors.	0.9	Fixed, assumed from reference [46].
$\boldsymbol{d_h}$	1/day	Death rate of SHIV-specific effector $CD8^+$ T cells.	0.05	Fitted.
$\boldsymbol{\frac{1}{\theta}}$	μL/cells	50% maximum value of SHIV-specific immune cells to block virus production.	1	Fixed.

358

References

1. Chun T-W, Carruth L, Finzi D, et al. Quantification of latent tissue reservoirs and total body viral load in HIV-1 infection. *Nature*. 1997;387(6629):183.

2. Chun T-W, Finzi D, Margolick J, Chadwick K, Schwartz D, Siliciano RF. In vivo fate of HIV-1-infected T cells: Quantitative analysis of the transition to stable latency. *Nature Medicine*. 1995;1(12):1284-1290.

3. Finzi D, Hermankova M, Pierson T, et al. Identification of a Reservoir for HIV-1 in Patients on Highly Active Antiretroviral Therapy. *Science*. 1997;278(5341):1295-1300.

4. Allers K, Hütter G, Hofmann J, et al. Evidence for the cure of HIV infection by CCR5Δ32/Δ32 stem cell transplantation. *Blood*. 2011;117(10):2791-2799.

5. Hütter G, Nowak D, Mossner M, et al. Long-Term Control of HIV by CCR5 Delta32/Delta32 Stem-Cell Transplantation. *New England Journal of Medicine*. 2009;360(7):692-698.

6. Gupta RK, Abdul-jawad S, McCoy LE, et al. HIV-1 remission following CCR5Δ32/Δ32 haematopoietic stem-cell transplantation. *Nature*. 2019:1.

7. Henrich TJ, Hanhauser E, Harrison LJ, et al. CCR5-Δ32 Heterozygosity, HIV-1 Reservoir Size, and Lymphocyte Activation in Individuals Receiving Long-term Suppressive Antiretroviral Therapy. *The Journal of Infectious Diseases*. 2016;213(5):766-770.

8. Henrich TJ, Hanhauser E, Marty FM, et al. Antiretroviral-Free HIV-1 Remission and Viral Rebound After Allogeneic Stem Cell Transplantation: Report of 2 Cases. *Annals of Internal Medicine*. 2014;161(5):319.

380 9. Henrich TJ, Hu Z, Li JZ, et al. Long-Term Reduction in Peripheral Blood HIV Type 1
381 Reservoirs Following Reduced-Intensity Conditioning Allogeneic Stem Cell Transplantation.
382 *The Journal of Infectious Diseases*. 2013;207(11):1694-1702.
383 10. Salgado M, Kwon M, Gálvez C, et al. Mechanisms That Contribute to a Profound
384 Reduction of the HIV-1 Reservoir After Allogeneic Stem Cell Transplant. *Annals of Internal*
385 *Medicine*. 2018.
386 11. Haworth KG, Peterson CW, Kiem H-P. CCR5-edited gene therapies for HIV cure:
387 Closing the door to viral entry. *Cytotherapy*. 2017;19(11):1325-1338.
388 12. Tebas P, Stein D, Tang WW, et al. Gene Editing of CCR5 in Autologous CD4 T Cells of
389 Persons Infected with HIV. *New England Journal of Medicine*. 2014;370(10):901-910.
390 13. Peterson CW, Wang J, Norman KK, et al. Long-term multilineage engraftment of
391 autologous genome-edited hematopoietic stem cells in nonhuman primates. *Blood*.
392 2016;127(20):2416-2426.
393 14. Peterson CW, Benne C, Polacino P, et al. Loss of immune homeostasis dictates SHIV
394 rebound after stem-cell transplantation. *JCI Insight*. 2017;2(4).
395 15. Peterson CW, Haworth KG, Polacino P, et al. Lack of viral control and development of
396 combination antiretroviral therapy escape mutations in macaques after bone marrow
397 transplantation. *Aids*. 2015;29(13):1597-1606.
398 16. Peterson CW, Wang J, Deleage C, et al. Differential impact of transplantation on
399 peripheral and tissue-associated viral reservoirs: Implications for HIV gene therapy. *PLOS*
400 *Pathogens*. 2018;14(4):e1006956.
401 17. Ho O, Larsen K, Polacino P, et al. Pathogenic infection of Macaca nemestrinawith a
402 CCR5-tropic subtype-C simian-human immunodeficiency virus. *Retrovirology*. 2009;6(1):65.

403 18. Jameson SC. Maintaining the norm: T-cell homeostasis. *Nature Reviews Immunology*.
404 2002;2(8):547-556.
405 19. Mehr R, Perelson AS. Blind T-cell homeostasis and the CD4/CD8 ratio in the thymus and
406 peripheral blood. *Journal of Acquired Immune Deficiency Syndromes and Human Retrovirology:*
407 *Official Publication of the International Retrovirology Association*. 1997;14(5):387-398.
408 20. Margolick JB, Donnenberg AD. T-cell homeostasis in HIV-1 infection. *Seminars in*
409 *Immunology*. 1997;9(6):381-388.
410 21. Schluns KS, Williams K, Ma A, Zheng XX, Lefrançois L. Cutting Edge: Requirement for
411 IL-15 in the Generation of Primary and Memory Antigen-Specific CD8 T Cells. *The Journal of*
412 *Immunology*. 2002;168(10):4827-4831.
413 22. Schluns KS, Kieper WC, Jameson SC, Lefrançois L. Interleukin-7 mediates the
414 homeostasis of naïve and memory CD8 T cells *in vivo*. *Nature Immunology*. 2000;1(5):426-432.
415 23. Goldrath AW, Luckey CJ, Park R, Benoist C, Mathis D. The molecular program induced
416 in T cells undergoing homeostatic proliferation. *Proceedings of the National Academy of*
417 *Sciences*. 2004;101(48):16885-16890.
418 24. Voehringer D, Liang H-E, Locksley RM. Homeostasis and Effector Function of
419 Lymphopenia-Induced "Memory-Like" T Cells in Constitutively T Cell-Depleted Mice. *The*
420 *Journal of Immunology*. 2008;180(7):4742-4753.
421 25. Boyman O, Létourneau S, Krieg C, Sprent J. Homeostatic proliferation and survival of
422 naïve and memory T cells. *European Journal of Immunology*. 2009;39(8):2088-2094.
423 26. Douek DC, Vescio RA, Betts MR, et al. Assessment of thymic output in adults after
424 haematopoietic stemcell transplantation and prediction of T-cell reconstitution. *The Lancet*.
425 2000;355(9218):1875-1881.

426 27. Douek DC, McFarland RD, Keiser PH, et al. Changes in thymic function with age and
427 during the treatment of HIV infection. *Nature*. 1998;396(6712):690-695.
428 28. Bender J, Mitchell T, Kappler J, Marrack P. Cd4+ T Cell Division in Irradiated Mice
429 Requires Peptides Distinct from Those Responsible for Thymic Selection. *Journal of*
430 *Experimental Medicine*. 1999;190(3):367-374.
431 29. Kieper WC, Jameson SC. Homeostatic expansion and phenotypic conversion of naïve T
432 cells in response to self peptide/MHC ligands. *Proceedings of the National Academy of Sciences*.
433 1999;96(23):13306-13311.
434 30. Sallusto F, Geginat J, Lanzavecchia A. Central Memory and Effector Memory T Cell
435 Subsets: Function, Generation, and Maintenance. *Annual Review of Immunology*.
436 2004;22(1):745-763.
437 31. Saout CL, Mennechet S, Taylor N, Hernandez J. Memory-like CD8+ and CD4+ T cells
438 cooperate to break peripheral tolerance under lymphopenic conditions. *Proceedings of the*
439 *National Academy of Sciences*. 2008;105(49):19414-19419.
440 32. Sprent J, Surh CD. Normal T cell homeostasis: the conversion of naive cells into
441 memory-phenotype cells. *Nature Immunology*. 2011;12(6):478-484.
442 33. Takeda S, Rodewald H-R, Arakawa H, Bluethmann H, Shimizu T. MHC Class II
443 Molecules Are Not Required for Survival of Newly Generated CD4+ T Cells, but Affect Their
444 Long-Term Life Span. *Immunity*. 1996;5(3):217-228.
445 34. Tanchot C, Lemonnier FA, Pérarnau B, Freitas AA, Rocha B. Differential Requirements
446 for Survival and Proliferation of CD8 Naïve or Memory T Cells. *Science*. 1997;276(5321):2057-
447 2062.

448 35. Fry TJ, Mackall CL. Interleukin-7: master regulator of peripheral T-cell homeostasis?
449 *Trends in Immunology*. 2001;22(10):564-571.
450 36. Tan JT, Dudl E, LeRoy E, et al. IL-7 is critical for homeostatic proliferation and survival
451 of naïve T cells. *Proceedings of the National Academy of Sciences*. 2001;98(15):8732-8737.
452 37. Yamaki S, Ine S, Kawabe T, et al. OX40 and IL-7 play synergistic roles in the
453 homeostatic proliferation of effector memory CD4+ T cells. *European Journal of Immunology*.
454 2014;44(10):3015-3025.
455 38. Guillaume T, Rubinstein DB, Symann M. Immune Reconstitution and Immunotherapy
456 After Autologous Hematopoietic Stem Cell Transplantation. *Blood*. 1998;92(5):1471-1490.
457 39. Spits H. Development of αβ T cells in the human thymus. *Nature Reviews Immunology*.
458 2002;2(10):760.
459 40. Berkowitz RD, Beckerman KP, Schall TJ, McCune JM. CXCR4 and CCR5 Expression
460 Delineates Targets for HIV-1 Disruption of T Cell Differentiation. *The Journal of Immunology*.
461 1998;161(7):3702-3710.
462 41. Bleul CC, Wu L, Hoxie JA, Springer TA, Mackay CR. The HIV coreceptors CXCR4 and
463 CCR5 are differentially expressed and regulated on human T lymphocytes. *Proceedings of the*
464 *National Academy of Sciences*. 1997;94(5):1925-1930.
465 42. Zaitseva MB, Lee S, Rabin RL, et al. CXCR4 and CCR5 on Human Thymocytes:
466 Biological Function and Role in HIV-1 Infection. *The Journal of Immunology*.
467 1998;161(6):3103-3113.
468 43. Buchholz VR, Flossdorf M, Hensel I, et al. Disparate Individual Fates Compose Robust
469 CD8+ T Cell Immunity. *Science*. 2013;340(6132):630-635.

470 44. Farber DL, Yudanin NA, Restifo NP. Human memory T cells: generation,
471 compartmentalization and homeostasis. *Nature Reviews Immunology*. 2014;14(1):24-35.
472 45. Kaech SM, Wherry EJ, Ahmed R. Effector and memory T-cell differentiation:
473 implications for vaccine development. *Nature Reviews Immunology*. 2002;2(4):251-262.
474 46. Borducchi EN, Cabral C, Stephenson KE, et al. Ad26/MVA therapeutic vaccination with
475 TLR7 stimulation in SIV-infected rhesus monkeys. *Nature*. 2016;540(7632):284.
476 47. De Boer RJ. Understanding the Failure of CD8+ T-Cell Vaccination against
477 Simian/Human Immunodeficiency Virus. *Journal of Virology*. 2007;81(6):2838-2848.
478 48. Hill AL, Rosenbloom DIS, Nowak MA, Siliciano RF. Insight into treatment of HIV
479 infection from viral dynamics models. *Immunological Reviews*. 2018;285(1):9-25.
480 49. Perelson AS. Modelling viral and immune system dynamics. *Nature Reviews*
481 *Immunology*. 2002;2(1):28-36.
482 50. Perelson AS, Essunger P, Cao Y, et al. Decay characteristics of HIV-1-infected
483 compartments during combination therapy. *Nature*. 1997;387(6629):188.
484 51. Reeves DB, Peterson CW, Kiem H-P, Schiffer JT. Autologous Stem Cell Transplantation
485 Disrupts Adaptive Immune Responses during Rebound Simian/Human Immunodeficiency Virus
486 Viremia. *Journal of Virology*. 2017;91(13):e00095-00017.
487 52. Wodarz D, Garg N, Komarova NL, et al. Kinetics of CLL cells in tissues and blood
488 during therapy with the BTK inhibitor ibrutinib. *Blood*. 2014;123(26):4132-4135.
489 53. Wodarz D, Nowak MA. Specific therapy regimes could lead to long-term immunological
490 control of HIV. *Proceedings of the National Academy of Sciences*. 1999;96(25):14464-14469.
491 54. Doitsh G, Cavrois M, Lassen KG, et al. Abortive HIV Infection Mediates CD4 T Cell
492 Depletion and Inflammation in Human Lymphoid Tissue. *Cell*. 2010;143(5):789-801.

493 55. Matrajt L, Younan PM, Kiem H-P, Schiffer JT. The Majority of CD4+ T-Cell Depletion
494 during Acute Simian-Human Immunodeficiency Virus SHIV89.6P Infection Occurs in
495 Uninfected Cells. *Journal of Virology*. 2014;88(6):3202-3212.
496 56. Lavielle M. Mixed Effects Models for the Population Approach: Models, Tasks, Methods
497 and Tools (ed 1 edition). Boca Raton: Chapman and Hall/CRC; 2014.
498 57. Burnham KP, Anderson DR. Model Selection and Multimodel Inference: A Practical
499 Information-Theoretic Approach (ed 2). New York: Springer-Verlag; 2002.
500 58. Elemans M, Basatena N-KSa, Klatt NR, Gkekas C, Silvestri G, Asquith B. Why Don't
501 CD8+ T Cells Reduce the Lifespan of SIV-Infected Cells In Vivo? *PLOS Computational*
502 *Biology*. 2011;7(9):e1002200.
503 59. Klatt NR, Shudo E, Ortiz AM, et al. CD8+ Lymphocytes Control Viral Replication in
504 SIVmac239-Infected Rhesus Macaques without Decreasing the Lifespan of Productively
505 Infected Cells. *PLOS Pathogens*. 2010;6(1):e1000747.
506 60. Wong JK, Strain MC, Porrata R, et al. In Vivo CD8+ T-Cell Suppression of SIV Viremia
507 Is Not Mediated by CTL Clearance of Productively Infected Cells. *PLOS Pathogens*.
508 2010;6(1):e1000748.
509 61. Shridhar V, Chen Y, Gupta P. The CD8 Antiviral Factor (CAF) can suppress HIV-1
510 transcription from the Long Terminal Repeat (LTR) promoter in the absence of elements
511 upstream of the CATATAA box. *Virology Journal*. 2014;11(1):130.
512 62. Blazek D, Teque F, Mackewicz C, Peterlin M, Levy JA. The CD8+ cell non-cytotoxic
513 antiviral response affects RNA polymerase II-mediated human immunodeficiency virus
514 transcription in infected CD4+ cells. *Journal of General Virology*. 2016;97(1):220-224.

515 63. Zhang L, Yu W, He T, et al. Contribution of Human α-Defensin 1, 2, and 3 to the Anti-
516 HIV-1 Activity of CD8 Antiviral Factor. *Science*. 2002;298(5595):995-1000.
517 64. Levy JA, Mackewicz CE, Barker E. Controlling HIV pathogenesis: the role of the
518 noncytotoxic anti-HIV response of CD8+ T cells. *Immunology Today*. 1996;17(5):217-224.
519 65. A. OA, J. PL. CD4+ T-cell depletion in HIV infection: mechanisms of immunological
520 failure. *Immunological Reviews*. 2013;254(1):54-64.
521 66. Douek DC, Picker LJ, Koup RA. T Cell Dynamics in HIV-1 Infection. *Annual Review of*
522 *Immunology*. 2003;21(1):265-304.
523 67. Okoye A, Meier-Schellersheim M, Brenchley JM, et al. Progressive CD4+ central–
524 memory T cell decline results in CD4+ effector–memory insufficiency and overt disease in
525 chronic SIV infection. *Journal of Experimental Medicine*. 2007;204(9):2171-2185.
526 68. Okoye AA, Rohankhedkar M, Abana C, et al. Naive T cells are dispensable for memory
527 CD4+ T cell homeostasis in progressive simian immunodeficiency virus infection. *Journal of*
528 *Experimental Medicine*. 2012;209(4):641-651.
529 69. Zhen A, Peterson CW, Carrillo MA, et al. Long-term persistence and function of
530 hematopoietic stem cell-derived chimeric antigen receptor T cells in a nonhuman primate model
531 of HIV/AIDS. *PLOS Pathogens*. 2017;13(12):e1006753.
532 70. Krenger W, Blazar BR, Holländer GA. Thymic T-cell development in allogeneic stem
533 cell transplantation. *Blood*. 2011;117(25):6768-6776.
534 71. Roux E, Dumont-Girard F, Starobinski M, et al. Recovery of immune reactivity after T-
535 cell–depleted bone marrow transplantation depends on thymic activity. *Blood*. 2000;96(6):2299-
536 2303.

537 72. Lapidot T, Dar A, Kollet O. How do stem cells find their way home? *Blood*.
538 2005;106(6):1901-1910.
539 73. Chute J. Stem cell homing. *Current Opinion in Hematology*. 2006;13(6):399-406.
540 74. Markowitz M, Louie M, Hurley A, et al. A Novel Antiviral Intervention Results in More
541 Accurate Assessment of Human Immunodeficiency Virus Type 1 Replication Dynamics and T-
542 Cell Decay In Vivo. *Journal of Virology*. 2003;77(8):5037-5038.
543 75. Cardozo EF, Andrade A, Mellors JW, Kuritzkes DR, Perelson AS, Ribeiro RM.
544 Treatment with integrase inhibitor suggests a new interpretation of HIV RNA decay curves that
545 reveals a subset of cells with slow integration. *PLOS Pathogens*. 2017;13(7):e1006478.
546 76. Chen HY, Mascio MD, Perelson AS, Ho DD, Zhang L. Determination of virus burst size
547 in vivo using a single-cycle SIV in rhesus macaques. *Proceedings of the National Academy of*
548 *Sciences*. 2007;104(48):19079-19084.
549 77. Ramratnam B, Bonhoeffer S, Binley J, et al. Rapid production and clearance of HIV-1
550 and hepatitis C virus assessed by large volume plasma apheresis. *The Lancet*.
551 1999;354(9192):1782-1785.
552

Figure Legends

Figure 1. Study design and mathematical modeling. A. Four animals were infected with SHIV, suppressed with cART and underwent TBI/HSPC transplantation without editing of CCR5 (Transplant group). A control group of four animals did not receive TBI or HSPC transplantation. Both groups underwent ATI approximately one year after cART initiation. **B.** Mathematical model for T cell reconstitution. Each circle represents a cell compartment: T represents the HSPCs from the transplant; P, the progenitor cells in bone marrow (BM) and Thymus; S and N, $CD4^+CCR5^+$ and $CD4^+CCR5^-$ T cells, respectively; M and E, the $CD8^+$ T cells with naïve and central memory phenotypes, and effector memory phenotypes, respectively. N cells come from the thymus at a rate λ_f, grow with maximum rate r_n, upregulate CCR5 at rate λ_n, and are cleared at rate d_n. S cells grow with maximum division rate r_s, downregulate CCR5 at a rate λ_s, and are cleared at rate d_s. M cells have thymic input of λ_e, grow with maximum division rate r_m, differentiate to effector memory at rate λ_m, and are cleared at rate d_m. The E compartment grows with maximum division rate r_e and is cleared at rate d_e. All $CD4^+$ and $CD8^+$ T cell subsets compete to grow logistically with same carrying capacity K. **C.** Mathematical model for virus dynamics. We adapted the previous model by including the following assumptions. Susceptible cells, S, are infected by the virus, V, at rate β. A fraction τ of the infected cells produce virus, I_p, and the other fraction become unproductively infected, I_u. All infected cells die at rate δ_I. I_P cells arise from activation of latently infected cells at rate ξL, produce virus at a rate π, that is cleared at rate γ. $CD8^+$ M cells proliferate in the presence of infection with rate ω_8 from which a fraction f become SHIV-specific $CD8^+$ effector T cells, E_h, that are removed at a rate d_h. These effector cells reduce virus production or infectivity by $1/(1+\theta E_h)$, or $1/(1+\varphi E_h)$, respectively. Non-

susceptible $CD4^+$ T cells upregulate CCR5 in the presence of infection and replenish the susceptible pool with rate ω_4.

Figure 2. $CD4^+$ and $CD8^+$ T cell dynamics post-transplantation, pre-ATI. A. $CD4^+CCR5^+$, **B.** $CD4^+CCR5^-$, and **C.** total $CD8^+$ T cells from animals in the control (blue) and transplant groups (red). **D.** Range of blood $CD4^+$ and $CD8^+$ T cell counts using all data points for the period before ATI in control animals (p-value calculated with a paired t-test for averaged measurements post-transplant). **E.** Distribution of the growth rate estimates of $CD4^+CCR5^+$, $CD4^+CCR5^-$, and $CD8^+$ T cells using all data points from time of transplant until their levels reached set point in transplanted animals (p-value calculated using a paired t-test). We assumed set point as the data point after which the sum of consecutive changes from the moment of transplant in T cell counts was smaller or equal to zero. **F.** Correlation between total $CD8^+$ T cell and $CD8^+$ T_{EM} cell counts for all data points post-transplant in transplanted animals (p-value computed using repeated measures correlation test).

Figure 3. Mathematical modeling of T cell reconstitution dynamics. A. Mathematical model that most parsimoniously explains the T cell reconstitution data. Each circle represents a cell compartment: *T* represents the HSPCs from the transplant; *P*, the progenitor cells in bone marrow (BM) and Thymus; *S* and *N*, $CD4^+CCR5^+$ and $CD4^+CCR5^-$ T cells, respectively; *M* and *E*, the $CD8^+$ T cells with naïve and central memory phenotypes, and effector memory phenotypes, respectively. **B-E:** Model predictions (black solid lines) vs. empirical data (red diamonds) for peripheral subset counts from animal A11200 in the transplant group. **B.** $CD4^+CCR5^+$, **C.** $CD4^+CCR5^-$, **D.** $CD8^+$ Total, **E.** $CD8^+$ T_{EM} and T_{naive}+T_{CM}. F. Model prediction

598 of the proliferation of $CD4^+CCR5^+$ T cells (solid line) and upregulation of CCR5 (dashed line)
599 over time for animal A11200.
600
601 **Figure 4. Plasma viral load and $CD4^+$ T cell kinetics after ATI. A.** Plasma viral loads, **B.**
602 peripheral blood $CD4^+CCR5^+$ T-cell counts, and **C.** $CD4^+CCR5^-$ T-cell counts from animals in
603 the control (blue) and transplant (red) groups, respectively. **D-G**: Distributions of **D.** peak viral
604 load post-ATI, **E.** viral load at endpoint necropsy, **F.** $CD4^+CCR5^+$ T-cell nadir post-ATI, **G.**
605 $CD4^+CCR5^-$ T-cell nadir post-ATI. P-values were calculated using Mann-Whitney test. **H.**
606 Correlations between plasma viral load and peripheral blood $CD4^+CCR5^+$ T-cells in each animal
607 post-ATI. Each panel shows the timepoints post-ATI for each animal. P-values in each panel
608 were calculated using Spearman's rank test for all time points post-ATI for the corresponding
609 animal.
610
611 **Figure 5. Mathematical modeling of virus and T cell kinetics during HSPC transplantation.**
612 **A.** Mathematical model that most parsimoniously describes the relationship between plasma viral
613 load and peripheral T-cell counts. $CD4^+CCR5^+$ T cells, S, are susceptible to the virus, V. Infected
614 cells are divided into those that are able to produce virus, I_p, or not, I_u. Precursor $CD8^+$ cells, M,
615 divide and differentiate in the presence of infected cells becoming SHIV-specific effector cells,
616 E_h. E_h cells reduce virus production by a factor of $1/(1+\theta E_h)$. The model assumes a constant
617 activation of latent cells, $\bar{L}$. **B.** Best fits of the model (black lines) to SHIV RNA, and blood
618 $CD4^+CCR5^+$ and $CD4^+CCR5^-$ T cell counts. Scatterplots of the SHIV-dependent CD8
619 proliferation rate (ω_8) vs. **C.** $CD4^+CCR5^+$ nadir, and **D.** final observed viral load from all
620 animals; (p-values calculated using Spearman's rank test). **E-F:** Individual parameter estimates

621 of **E.** the SHIV-dependent CD8 proliferation rate (ω_8) and **F.** the time of rebound after ATI (see
622 text). Blue: control, and red: transplant groups (p-values calculated by Mann-Whitney test).
623
624 **Figure 6. Model predictions for post-rebound viral control after CCR5 gene-edited HSPC**
625 **transplant. A.** Schematic of the extended mathematical model that now includes CCR5-edited,
626 protected cells. Now, protected cells from transplant: T_p, protected progenitor cells in bone
627 marrow/thymus: P_p, and protected $CD4^+CCR5^-$ T cells: N_p are included. The initial fraction of
628 protected cells is represented by the parameter f_p. **B.** Predictions for plasma viral load up to one
629 year post-ATI using the adapted model for varying values of f_p (using parameter estimates from
630 animal Z09144). **C-F.** Predictions for plasma viral load (heat-map color) for each animal at a
631 given time post-ATI (x-axis) and a given f_p (y-axis). **G-H.** Predicted maximum decrease of
632 $CD4^+CCR5^+$ T cells during the first 10 weeks after ATI for the minimum fraction of protected
633 cells required to obtain post-rebound control after 2 years using parameter estimates for each
634 animal with (**G.**) and without (**H.**) measurement error.
635
636

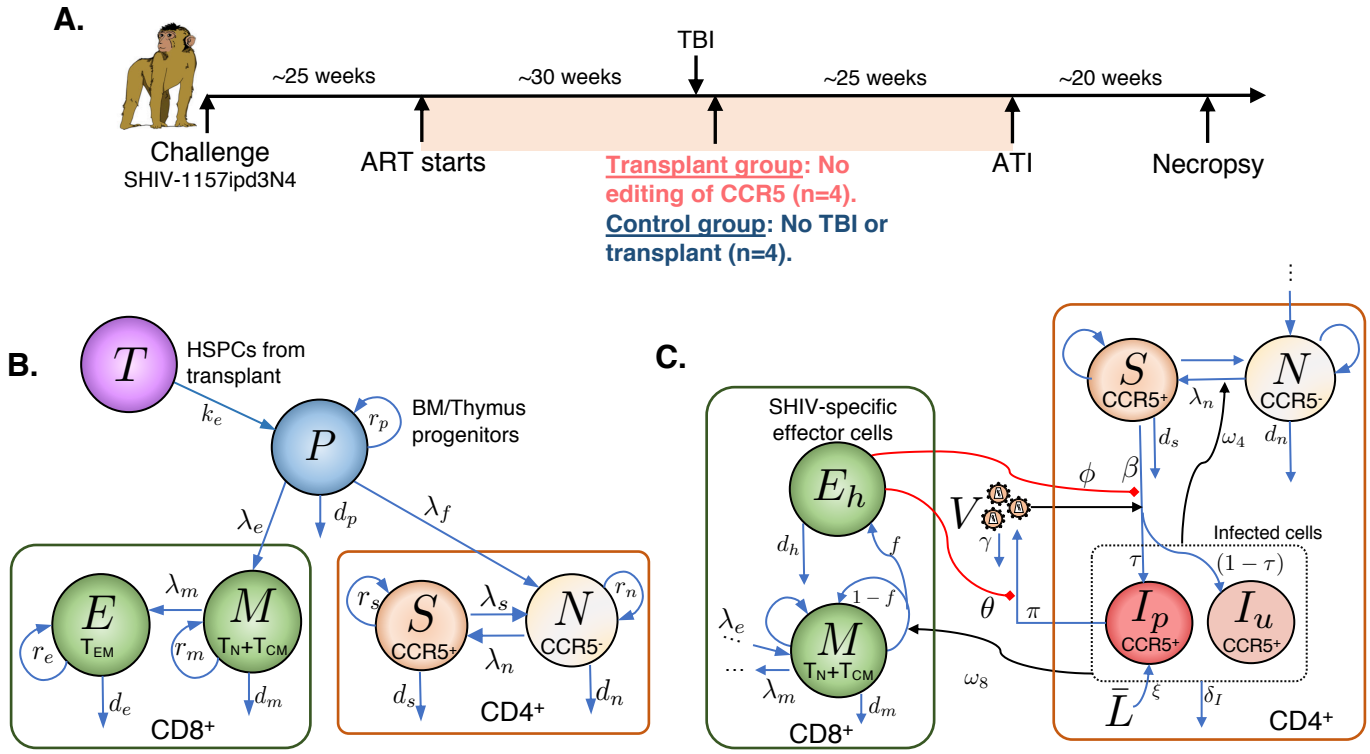

Figure 1. Study design and mathematical modeling. A. Four animals were infected with SHIV, suppressed with cART and underwent TBI/HSPC transplantation without editing of CCR5 (Transplant group). A control group of four animals did not receive TBI or HSPC transplantation. Both groups underwent ATI approximately one year after cART initiation. **B.** Mathematical model for T cell reconstitution. Each circle represents a cell compartment: T represents the HSPCs from the transplant; P, the progenitor cells in bone marrow (BM) and Thymus; S and N, CD4$^+$CCR5$^+$ and CD4$^+$CCR5$^-$ T cells, respectively; M and E, the CD8$^+$ T cells with naïve and central memory phenotypes, and effector memory phenotypes, respectively. N cells come from the thymus at a rate λ_f, grow with maximum rate r_n, upregulate CCR5 at rate λ_n, and are cleared at rate d_n. S cells grow with maximum division rate r_s, downregulate CCR5 at a rate λ_s, and are cleared at rate d_s. M cells have thymic input of λ_e, grow with maximum division rate r_m, differentiate to effector memory at rate λ_m, and are cleared at rate d_m. The E compartment grows with maximum division rate r_e and is cleared at rate d_e. All CD4$^+$ and CD8$^+$ T cell subsets compete to grow logistically with same carrying capacity K. **C.** Mathematical model for virus dynamics. We adapted the previous model by including the following assumptions. Susceptible cells, S, are infected by the virus, V, at rate β. A fraction τ of the infected cells produce virus, I_p, and the other fraction become unproductively infected, I_u. All infected cells die at rate δ_I. I_P cells arise from activation of latently infected cells at rate ξL, produce virus at a rate π, that is cleared at rate γ. CD8$^+$ M cells proliferate in the presence of infection with rate ω_8 from which a fraction f become SHIV-specific CD8$^+$ effector T cells, E_h, that are removed at a rate d_h. These effector cells reduce virus production or infectivity by $1/(1+\theta E_h)$, or $1/(1+\phi E_h)$, respectively. Non-susceptible CD4$^+$ T cells upregulate CCR5 in the presence of infection and replenish the susceptible pool with rate ω_4.

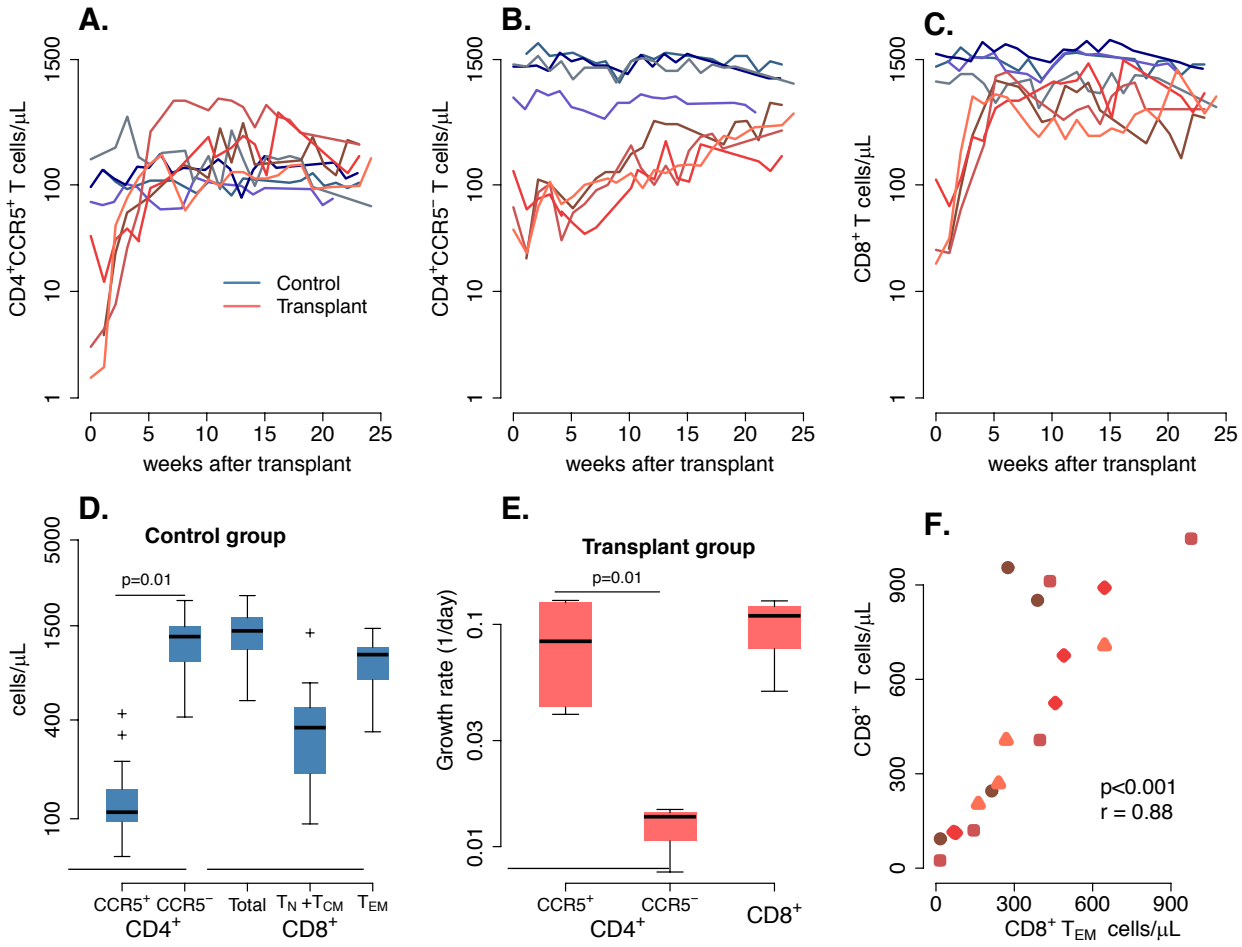

Figure 2. CD4⁺ and CD8⁺ T cell dynamics post-transplantation, pre-ATI. A. $CD4^+CCR5^+$, **B.** $CD4^+CCR5^-$, and **C.** total $CD8^+$ T cells from animals in the control (blue) and transplant groups (red). **D.** Range of blood $CD4^+$ and $CD8^+$ T cell counts using all data points for the period before ATI in control animals (p-value calculated with a paired t-test for averaged measurements post-transplant). **E.** Distribution of the growth rate estimates of $CD4^+CCR5^+$, $CD4^+CCR5^-$, and $CD8^+$ T cells using all data points from time of transplant until their levels reached set point in transplanted animals (p-value calculated using a paired t-test). We assumed set point as the data point after which the sum of consecutive changes from the moment of transplant in T cell counts was smaller or equal to zero. **F.** Correlation between total $CD8^+$ T cell and $CD8^+$ T_{EM} cell counts for all data points post-transplant in transplanted animals (p-value computed using repeated measures correlation test).

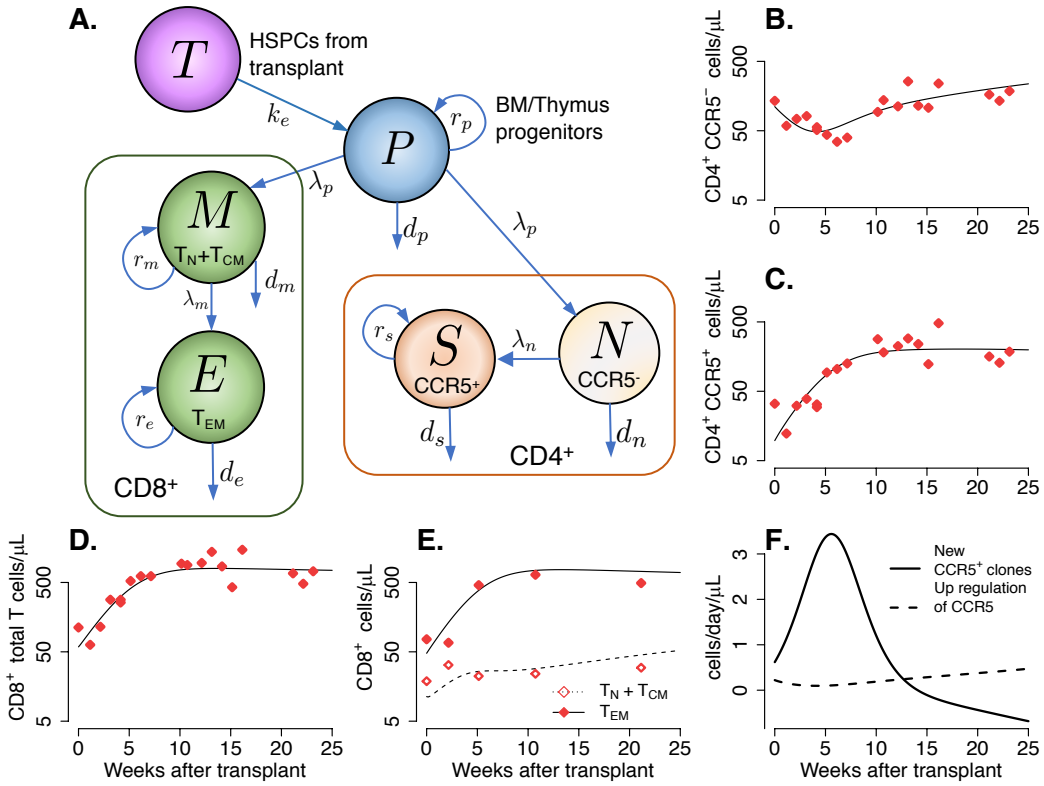

Figure 3. Mathematical modeling of T cell reconstitution dynamics. A. Mathematical model that most parsimoniously explains the T cell reconstitution data. Each circle represents a cell compartment: *T* represents the HSPCs from the transplant; *P*, the progenitor cells in bone marrow (BM) and Thymus; *S* and *N*, $CD4^+CCR5^+$ and $CD4^+CCR5^-$ T cells, respectively; *M* and *E*, the $CD8^+$ T cells with naïve and central memory phenotypes, and effector memory phenotypes, respectively. **B-E**: Model predictions (black solid lines) vs. empirical data (red diamonds) for peripheral subset counts from animal A11200 in the transplant group. **B.** $CD4^+CCR5^+$, **C.** $CD4^+CCR5^-$, **D.** $CD8^+$ Total, **E.** $CD8^+$ T_{EM} and T_{naive}+T_{CM}. **F.** Model prediction of the proliferation of $CD4^+CCR5^+$ T cells (solid line) and upregulation of CCR5 (dashed line) over time for animal A11200.

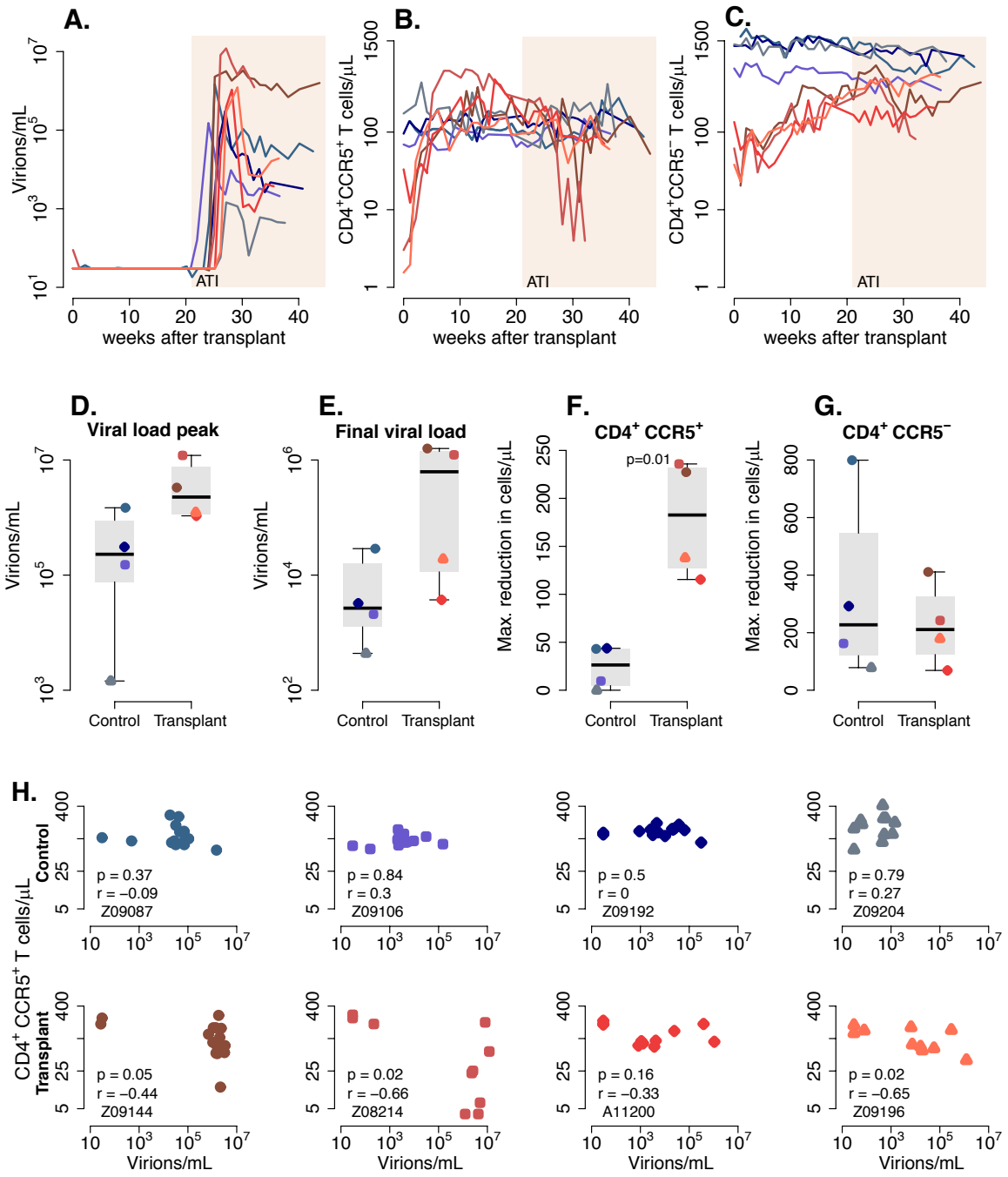

Figure 4. Plasma viral load and CD4⁺ T cell kinetics after ATI. A. Plasma viral loads, **B.** peripheral blood CD4⁺CCR5⁺ T-cell counts, and **C.** CD4⁺CCR5⁻ T-cell counts from animals in the control (blue) and transplant (red) groups, respectively. **D-G**: Distributions of **D.** peak viral load post-ATI, **E.** viral load at endpoint necropsy, **F.** CD4⁺CCR5⁺ T-cell nadir post-ATI, **G.** CD4⁺CCR5⁻ T-cell nadir post-ATI. P-values were calculated using Mann-Whitney test. **H.** Correlations between plasma viral load and peripheral blood CD4⁺CCR5⁺ T-cells in each animal post-ATI. Each panel shows the timepoints post-ATI for each animal. P-values in each panel were calculated using Spearman's rank test for all time points post-ATI for the corresponding animal.

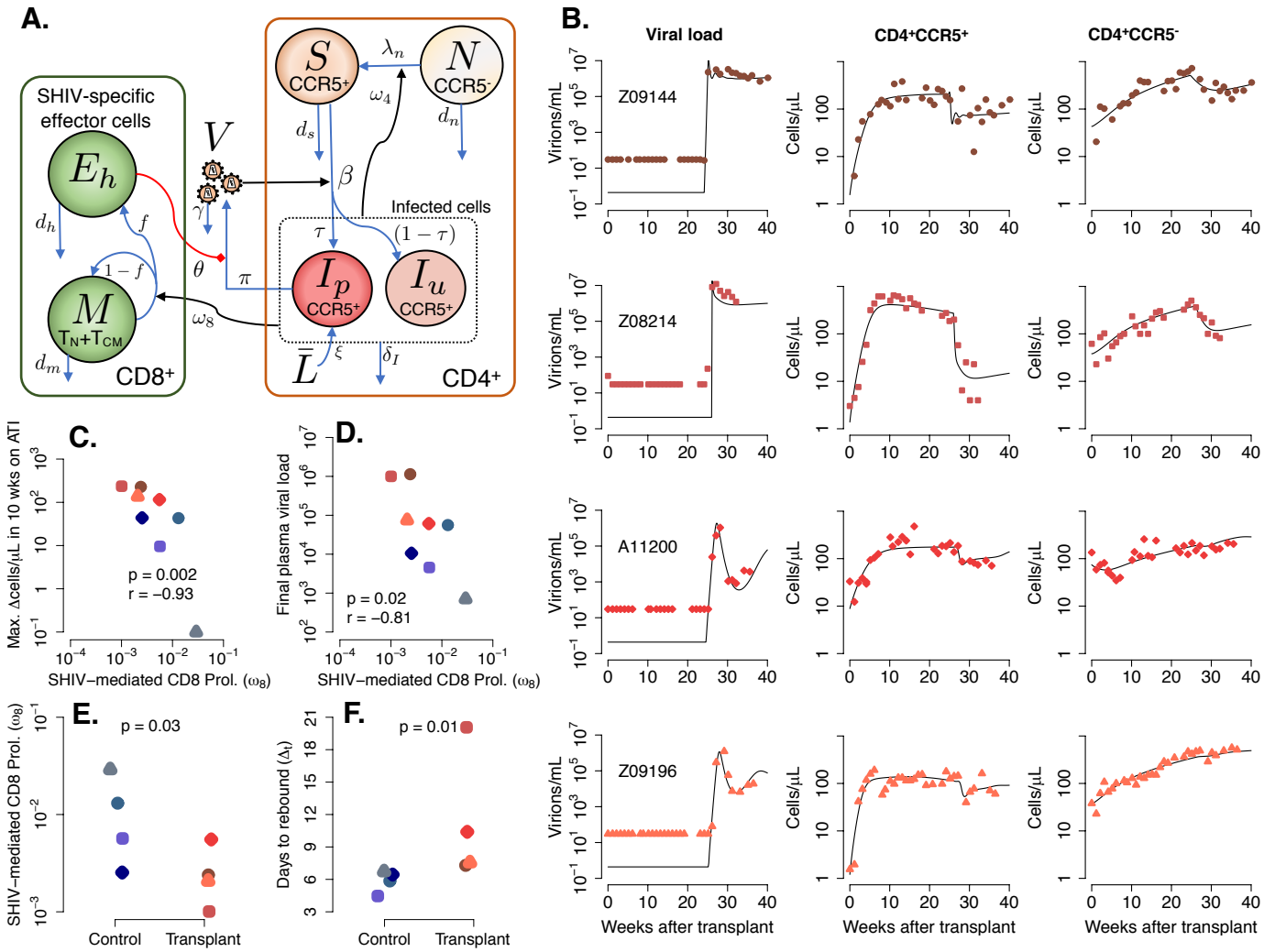

Figure 5. Mathematical modeling of virus and T cell kinetics during HSPC transplantation. A. Mathematical model that most parsimoniously describes the relationship between plasma viral load and peripheral T-cell counts. CD4+CCR5+ T cells, *S*, are susceptible to the virus, *V*. Infected cells are divided into those that are able to produce virus, I_p, or not, I_u. Precursor CD8+ cells, *M*, divide and differentiate in the presence of infected cells becoming SHIV-specific effector cells, E_h. E_h cells reduce virus production by a factor of $1/(1+\theta E_h)$. The model assumes a constant activation of latent cells, $\bar{L}$. **B.** Best fits of the model (black lines) to SHIV RNA, and blood CD4+CCR5+ and CD4+CCR5- T cell counts. Scatterplots of the SHIV-dependent CD8 proliferation rate (ω_8) vs. **C.** CD4+CCR5+ nadir, and **D.** final observed viral load from all animals; (p-values calculated using Spearman's rank test). **E-F**: Individual parameter estimates of **E.** the SHIV-dependent CD8 proliferation rate (ω_8) and **F.** the time of rebound after ATI (see text). Blue: control, and red: transplant groups (p-values calculated by Mann-Whitney test).

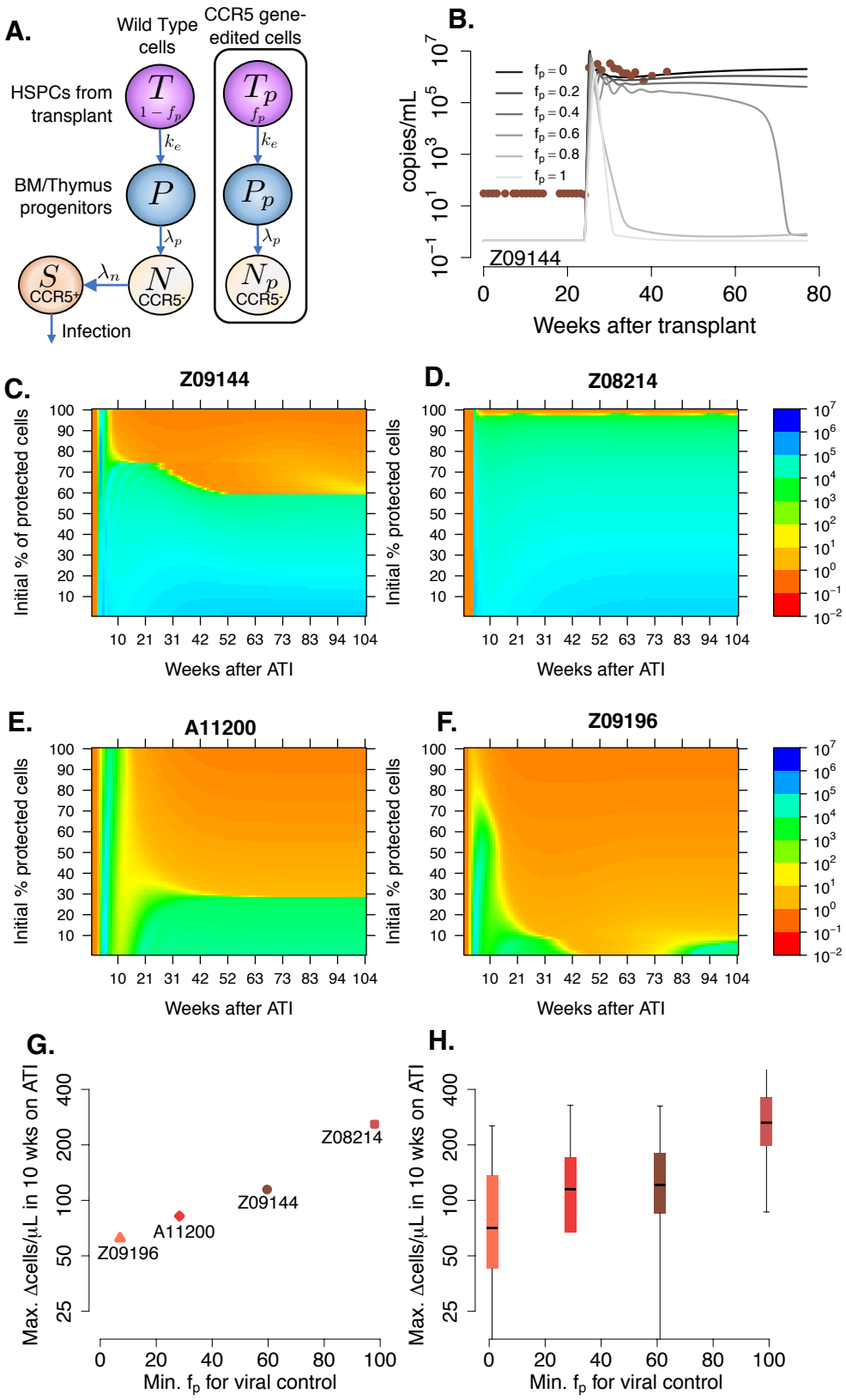
A.
Wild Type cells
CCR5 gene-edited cells
HSPCs from transplant
BM/Thymus progenitors
Infection
B.
copies/mL
Z09144
Weeks after transplant
C.
Z09144
Initial % of protected cells
Weeks after ATI
D.
Z08214
E.
A11200
F.
Z09196
G.
Max. Δcells/μL in 10 wks on ATI
Min. f_p for viral control
H.

Figure 6. Model predictions for post-rebound viral control after CCR5 gene-edited HSPC transplant. A. Schematic of the extended mathematical model that now includes CCR5-edited, protected cells. Now, protected cells from transplant: T_p, protected progenitor cells in bone marrow/thymus: P_p, and protected $CD4^+CCR5^-$ T cells: N_p are included. The initial fraction of protected cells is represented by the parameter f_p. **B.** Predictions for plasma viral load up to one year post-ATI using the adapted model for varying values of f_p (using parameter estimates from animal Z09144). **C-F.** Predictions for plasma viral load (heat-map color) for each animal at a given time post-ATI (x-axis) and a given f_p (y-axis). **G-H.** Predicted maximum decrease of $CD4^+CCR5^+$ T cells during the first 10 weeks after ATI for the minimum fraction of protected cells required to obtain post-rebound control after 2 years using parameter estimates for each animal with (**G.**) and without (**H.**) measurement error.